

1 Study of time resolution of low-gain avalanche detectors

2 Kyoji Onaru¹, Kazuhiko Hara¹, Daigo Harada¹, Sayaka Wada¹,
3 Koji Nakamura², Yoshinobu Unno²

4 ¹*University of Tsukuba, Tsukuba, Ibaraki 305-8571, Japan*

5 ²*High Energy Accelerator Research Organization (KEK), Tsukuba, Ibaraki 305-0801,*
6 *Japan*

7 **Abstract**

Low Gain Avalanche Detector (LGAD) is a semiconductor device that amplifies signals inside the sensor using avalanche mechanism. As the multiplication occurs in a thin p-n junction, it can achieve a superior time resolution, e.g., 30 ps as obtained in our previous beam-test study. In combined with excellent 3-D spatial information achievable with semiconductor devices, we are targeting to realize a 4-D detector. Although high-energy beams are very useful in evaluating the time resolution of the LGAD, desk-top measurement systems are very helpful for quick evaluation of LGAD samples under development. We are, therefore, developing a time measurement system using β -rays from a ⁹⁰Sr source. We obtained a time resolution slightly degraded but similar to the beam-test results. In realizing a 4-D detector, readout needs to be finely segmented with keeping the gain uniform in wider area. As a device with such segmentation, we studied AC-LGAD in which a gain layer is implanted over the entire area of the sensor and the signal is read out by segmented AC pads interleaved with an insulating layer. Several AC-LGAD structures were created in a TCAD simulation, and optimal sensor design parameters were extracted.

8 *Keywords:* 4D detector, segmented LGAD, AC-LGAD

9 **1. Introduction**

10 The Low Gain Avalanche Detector (LGAD) is a semiconductor detector
11 implemented with avalanche mechanism for signal amplification. Figure 1

12 illustrates a typical LGAD structure. In an conventional n-in-p type silicon
13 semiconductor detector, LGAD has a p^+ well implanted under the n^{++}
14 readout implant with the p-type impurity concentration higher than that
15 in the bulk. The junction at the p^+-n^{++} interface acts as the gain layer
16 creating a high electric field sufficient to initiate avalanche multiplication.
17

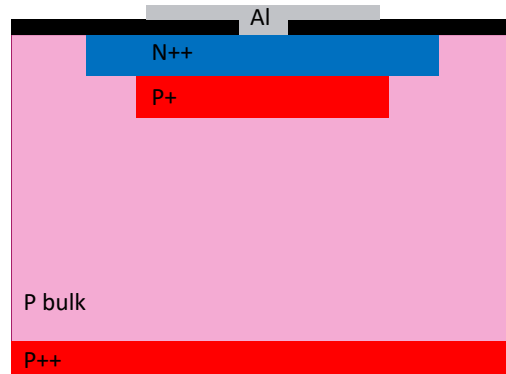


Figure 1: Typical LGAD structure.

18 Main contributors degrading the time resolution are the time walk and
19 time jitter [1], [2]. The time walk is a fluctuation of the timing exceeding the
20 threshold and is caused by the variation in signal magnitude. The time walk
21 decreases for faster signals with larger signal slope dV/dt . The time jitter
22 is caused by the signal noise and is smaller for the device with better S/N
23 ratio. The LGAD amplifies the signal in the vicinity of the readout electrode
24 and hence makes the signal rise faster. The S/N ratio is maximized for low
25 amplification gain of around ten where the signal is amplified sufficiently
26 while the noise amplification is only partial. As the LGAD meets these

27 conditions, good time resolution is achievable.

28 The 4-D detector measures the traversing charge particle four-dimensionally
29 providing time information in addition to the 3-D position information. The
30 big challenge for the particle tracker in future accelerator experiments is to
31 deal with the increased pile-up events associated with increasing the accel-
32 erator luminosity. The time information of e.g., 30 ps as reported in [5],
33 corresponding to 10 mm in space, is possible to narrow down the candidate
34 hits to be considered for tracking, which would be very effective in recon-
35 structing tracks in high pile-up environment as envisaged in future hadron
36 collider experiments. The additional time information helps reduce the can-
37 didate hits, which would reduce the computational load greatly and would
38 change the strategy of tracking.

39

40 **2. Desk-top time resolution measurement system**

41 The time resolution of LGADs has been measured in beam experiments
42 using large accelerators. We are aiming to develop a desk-top measurement
43 system that allows us evaluating the time resolution much more easily. The
44 system uses a ^{90}Sr β source with the signals read out with flash ADCs,
45 as illustrated in Fig. 2. Two sensors were placed on top of the other, and
46 the bottom sensor was used as triggering β rays. The sensors were $2 \times$
47 2 array of 1.3 mm square pads being evaluated for the CMS experiment
48 [4]. The amplifier board based on wide-band (DC to 3 GHz) InGaP HBT
49 MMIC amplifier chips [4] was home-made. The waveforms are digitized with
50 flash ADCs (CAEN DT5742) at 5 GHz sampling with 12-bit ADCs covering

51 $V_{pp} = \pm 1$ V range. Events are read out when the bottom sensor showed
 52 large signal exceeding a preset voltage. The sensors mounted on the amplifier
 53 board were placed in a thermostat chamber to control the temperature at
 54 -20 °C

55

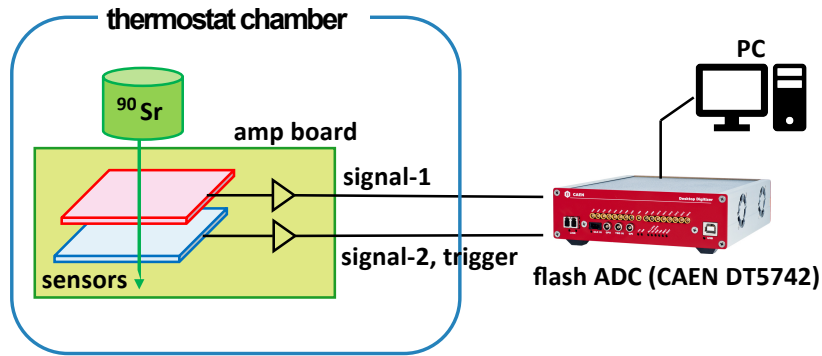


Figure 2: Setup for timing measurements.

56 Figure 3 shows the distribution of the event-by-event maximum ADCs in
 57 the two waveforms (ADC_up and ADC_dwn). As the bottom LGAD signal
 58 was used for the event trigger, the pedestal is only seen for the top LGAD.
 59 The large population around $(\text{ADC}_{\text{up}}, \text{ADC}_{\text{dwn}}) = (300, 300)$ corresponds
 60 to the case both sensors detect penetrating β rays. In the following, we
 61 require the difference of the times at the maximum to be within 5 ns as the
 62 two sensors are only a few millimeters apart.

63

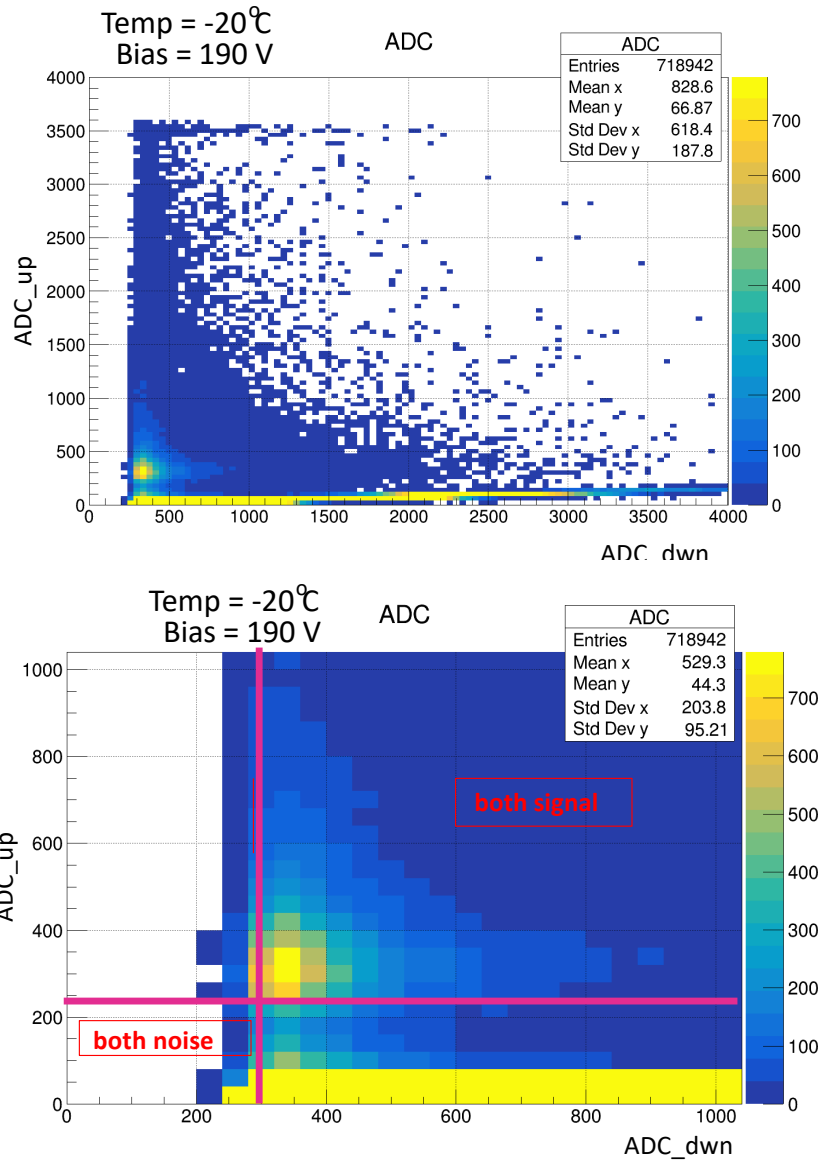


Figure 3: Correlation of maximal ADC values per event (top) in whole range, and (bottom) its expansion showing ADC < 1000.

64 After removing the noise events, fitting was performed using a quintic
 65 function as an example shown in Fig. 4. Using the fitted function, the time

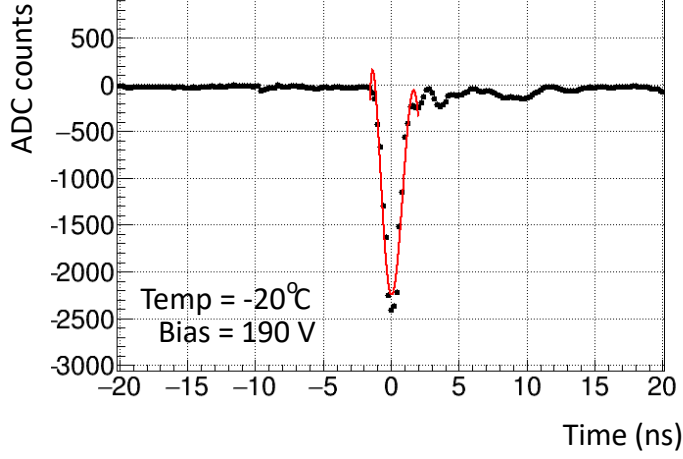


Figure 4: Waveform example of one LGAD signal, fitted with a quintic function.

66 at exceeding the threshold $V_{\text{threshold}} = V_{\text{max}} \times f$ was derived with varying
 67 the fraction f in the range $0 < f < 1$. The time was calculated for each of
 68 the two sensors using the same f value. The distribution of time difference
 69 as obtained in Fig. 5 was fitted with a Gaussian function. The obtained
 70 Gaussian σ can be written as

$$\sigma = \sqrt{\sigma(T_1)^2 + \sigma(T_2)^2}, \quad (1)$$

71 where the intrinsic time resolution of the two sensors is $\sigma(T_1)$ and $\sigma(T_2)$.
 72 As the tested LGADs are identical in design and were operated at the same
 73 bias voltage, we can assume that the two sensors have the same intrinsic
 74 time resolution. Therefore, the intrinsic time resolution of one LGAD can
 75 be calculated as

$$\sigma(T) = \sigma/\sqrt{2}. \quad (2)$$

76 Figure 6 shows the dependence of the time resolution on the fraction

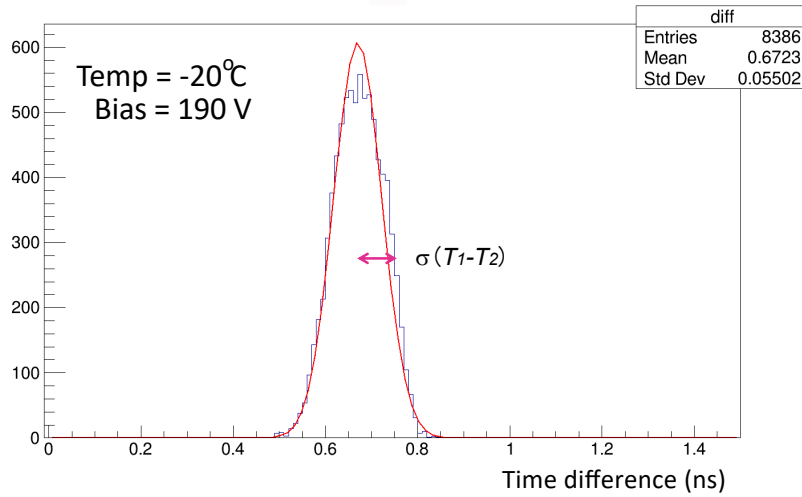


Figure 5: Distribution of time differences, fitted with a Gaussian function.

77 factor f .

78

79 Figure 7 shows the time resolution with respect to the reverse bias volt-
 80 age. Up to a bias voltage of -200V, the time resolution improves with the
 81 voltage, which is considered to be due to an increase in the amplification
 82 factor. On the other hand, at higher voltages, the time resolution deterio-
 83 rates, which is considered to be due to the gain being too large and to the
 84 S/N ratio degradation.

85

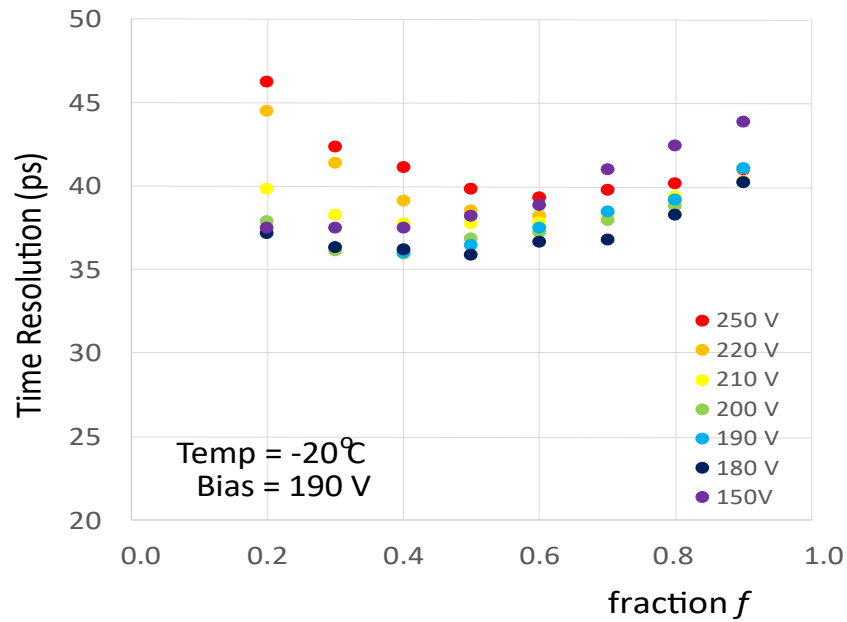


Figure 6: Time resolution as a function of threshold factor. The data points for several bias voltages are plotted.

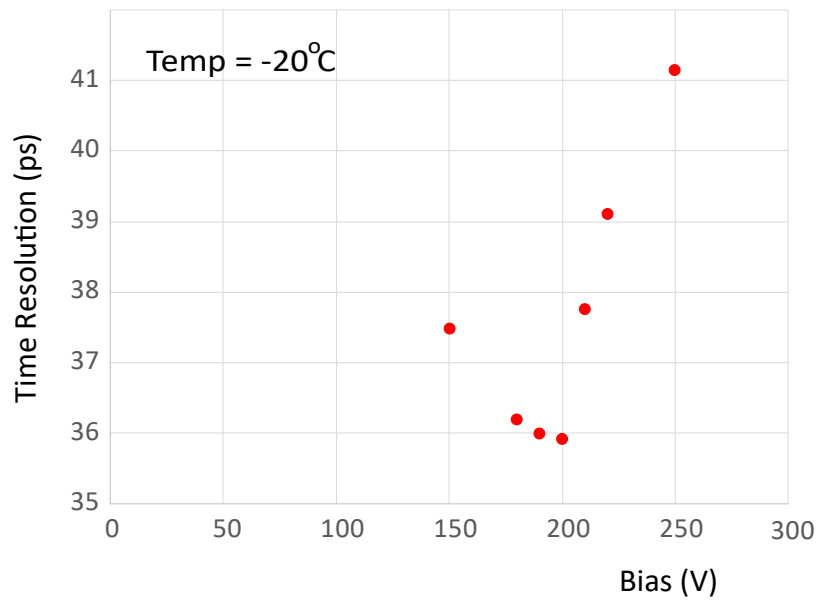


Figure 7: Time resolution as a function of bias voltage for $f=0.5$.

86 **3. AC-LGAD TCAD simulation**

87 The gain non-uniformity in a conventional strip-type LGAD structure
88 [3] is caused by the limited coverage of the n^{++} and p^+ gain layer. In AC-
89 LGAD the gain layer is made uniform covering the entire sensitive area while
90 readout segmentation is achieved by AC coupled electrodes. The primary
91 challenge in designing an AC-LGAD is the optimization of the n^{++} layer
92 resistivity. In order to prevent charges escaping to the ground, the n^{++}
93 implant impedance needs to be large enough, which may in turn result in
94 insufficient achievable gain. Also, if the resistance is too high, the collected
95 charge will not escape causing the sensor to charge up. The n^{++} concentra-
96 tion determines the degree of signal spread to the nearby readout electrodes,
97 which is also to be optimized at the same time. Another challenge concerns
98 about the gain. For n^{++} implanted with a lower concentration than stan-
99 dard, it is necessary to increase the p^+ concentration in stead so as to achieve
100 the similar gain. On the other hand, for excessively high p^+ concentration,
101 the sensor will break down before achieving sufficient gain.

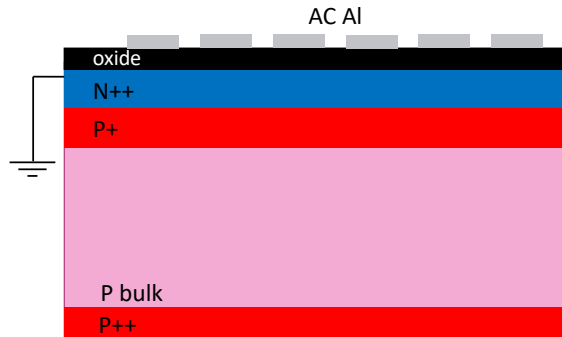


Figure 8: AC-LGAD structure.

102 An AC-LGAD structure shown in Fig. 9 was created using a TCAD [6],
 103 [3] simulation where p^+ and n^{++} gain layers were implanted covering the
 104 entire area of a $50\ \mu\text{m}$ thick p-type bulk. The AC coupled Al electrodes
 105 were created on top of an oxide film. In this simulation, only five AC-Al
 106 electrodes were placed for simplicity. The simulation is two dimensional, and
 107 AC-Al pitch and width are $80\ \mu\text{m}$ and $40\ \mu\text{m}$, respectively. For the reverse
 108 bias voltage, a negative voltage is applied to the p^{++} layer created on the
 109 back of the sensor, and the n^{++} electrode layer is grounded. The oxide film
 110 was trimmed out near the ends where DC-Al electrodes are contacted for
 111 grounding the n^{++} electrode.

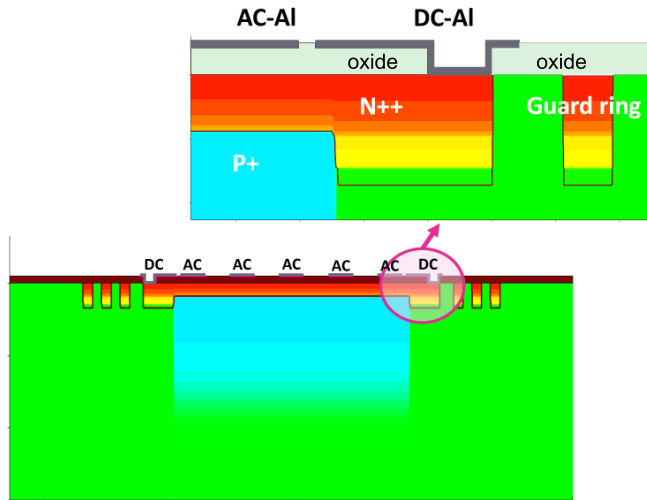


Figure 9: An AC-LGAD structure implemented in TCAD. Structure around the n^{++} electrode end is shown in the enlarged view.

112 Figures 10 and 11 show simulation results of the signal shape induced
 113 on each electrode up to the next-to-next electrode when MIP (minimum
 114 ionizing particles) is incident on the center on an electrode. Fig. 10 includes

115 the sets of signal shapes for the three n^{++} concentrations, showing that a
 116 50% change of n^{++} concentration affects significantly on the signal spread.
 117 An effect is seen that the charges initially move toward the AC-Al electrode
 118 giving positive signal then move away to the neighbors swinging the signal
 119 negatively. On the other hand, for the increased n^{++} concentration, the
 120 n^{++} resistivity is too low so that certain fraction of the charges flows to
 121 the neighboring electrodes, giving significant signal to the next electrodes.
 122 Contrarily, the signal will not be seen on the neighbors if the resistivity
 123 is too high as for the decreased n^{++} concentration. The signal sharing
 124 seems acceptable for this case, but since the charge movement towards the
 125 neighbors and finally to the DC-Al electrode is limited, the charges may stay
 126 below the AC-Al electrode.

127

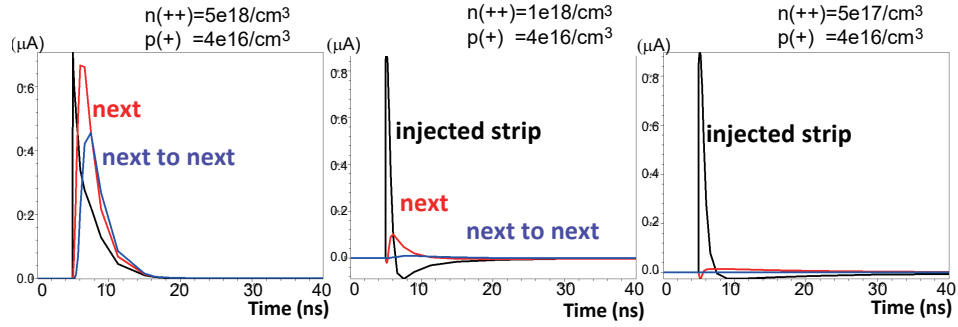


Figure 10: Signal shapes induced on the injected, next and next-to-next strips for three n^{++} concentrations.

128 Figure 11 shows the induced signal shape for two n^{++} thicknesses. Be-
 129 cause the resistance is reduced for thicker n^{++} , the negative signal swing is
 130 more enhanced.

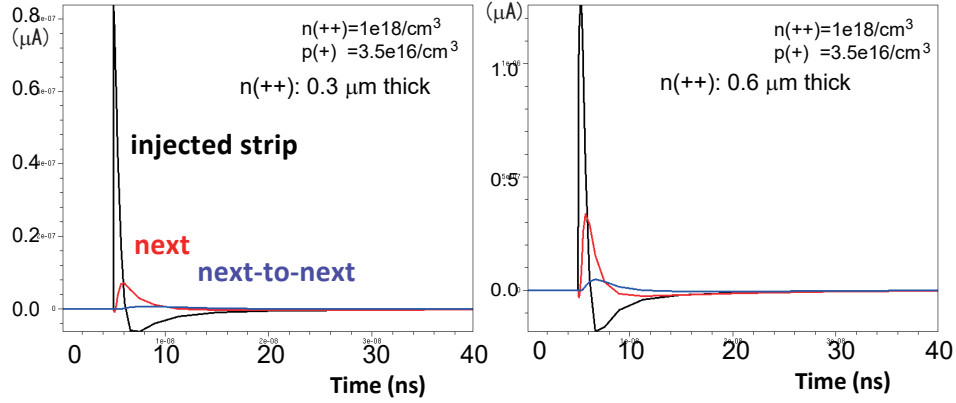


Figure 11: Signal shapes induced on the injected, next and next-to-next strips for two n^{++} thicknesses.

131 Figure 12 shows the simulation results of the gain at 300 V bias as a
 132 function of p^+ concentration plotted for various n^{++} concentrations. Here
 133 the gain is of the strip to which MIP was injected at its center, and the
 134 corresponding charge is the induced current integrated while the current is
 135 positive. The gain tends to increase with increasing p^+ and n^{++} concentra-
 136 tions up to some points. For achieving a gain of 10, $p^+ = 5 \times 10^{16} \text{ cm}^{-3}$
 137 and $n^{++} = 1 \times 10^{18} \text{ cm}^{-3}$ are the parameters.

138 Figure 13 shows the gain uniformity across the strips calculated for the
 139 concentration conditions given above and at 300 V bias. About 70% of the
 140 charge is collected to the incident electrode when the particle is incident at
 141 its center. The charge sum is fairly flat across the strips, indicating uniform
 142 gain is obtainable.

143

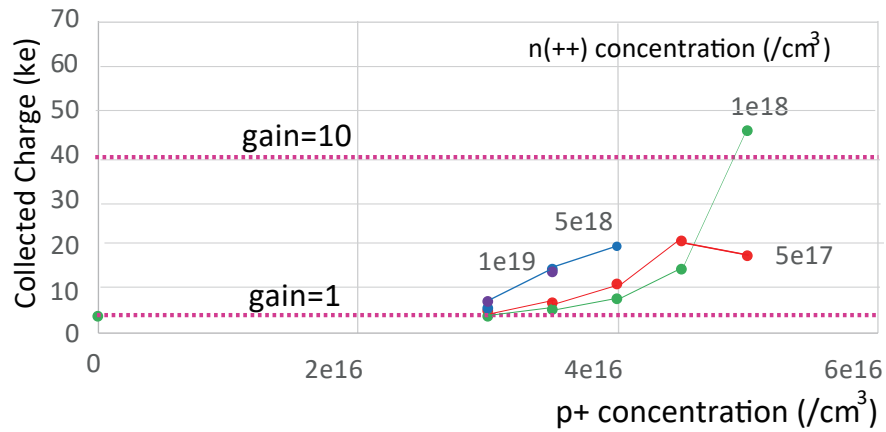


Figure 12: Gain at 300 V bias is plotted as a function of p^+ concentration. The values attached to the curves are n^{++} concentrations.

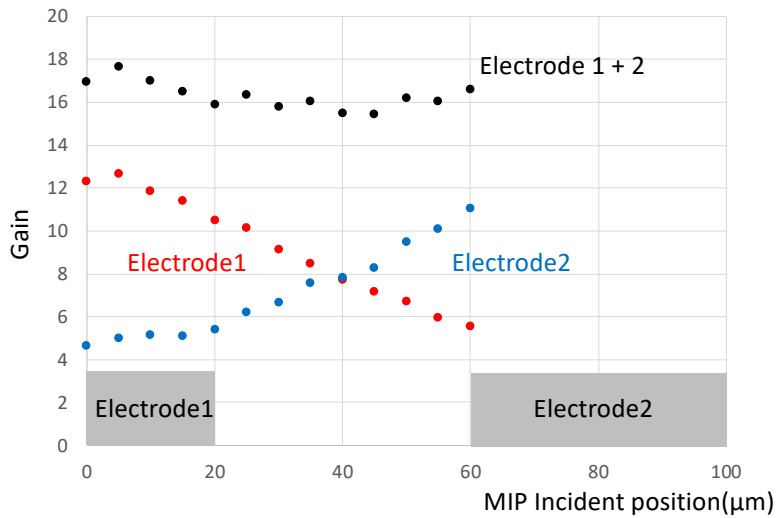


Figure 13: Gain uniformity across the strips.

144 **4. Conclusion**

145 We are developing LGAD sensors to realize a 4-D particle detector for
146 future accelerator experiments. Such a device should also be interesting
147 in new applications in medical equipment such as TOF-PET and in bio-
148 sciences. We reported a desk-top time resolution measurement system using
149 a β -ray source, confirming that the system is useful for quick time reso-
150 lution evaluation. We also performed a TCAD simulation for designing a
151 segmented AC-LGAD, and conclude that uniform and sufficient gain are
152 obtainable. Prototype AC-LGAD sensors are to be fabricated based on the
153 present study.

154 **5. Acknowledgments**

155 This research was supported in part by KAKENHI 19H04393 and US-
156 Japan Science and Technology Cooperation Program (2018-2019). Collab-
157 oration with Dr. A. Apresyan of FNAL who provided the amplifier circuit
158 design has been very fruitful and inevitable in carrying out the present study.
159 The discussions with K. Yamamura and S. Kamata of Hamamatsu Photonics
160 were very inspiring in designing the AC-LGAD.

161 **6. References**

162 **References**

- 163 [1] Hartmut F-W Sadrozinski, A. Seiden, N. Cartiglia, “4D tracking with ultra-
164 fast silicon detectors”, Rep. Prog. Phys. 81 026101(2018).

- 165 [2] N. Cartiglia, et. al., “Timing layers, 4- and 5-dimension tracking”. Nucl. In-
166 strument. and Meth. A924 (2019) 350-354.
- 167 [3] S. Wada, et al., “Design of a segmented LGAD sensor for development of a
168 4-D tracking detector”. poster presented at the 28th Int. Workshop on Vertex
169 Detectors VERTEX2019”, 13-18 October 2019, Lopud, Croatia.
- 170 [4] A. Apresyan, private communication (2019).
- 171 [5] S. Wada, et al., “Evaluation of characteristics of Hamamatsu low-gain
172 avalanche detectors”, Nucl. Instrum. and Meth. A924 (2019) 380-386.
- 173 [6] TCAD synopsis, homepage: <https://www.synopsys.com/>.